Biochimica et Biophysica Acta 1840 (2014) 2192–2202

Contents lists available at ScienceDirect

Biochimica et Biophysica Acta

journal homepage: www.elsevier.com/locate/bbagen

Time evolution of noise induced oxidation in outer hair cells: Role of NAD(P)H and plasma membrane fluidity

Giuseppe Maulucci [a], Diana Troiani [b,*], Sara Letizia Maria Eramo [b], Fabiola Paciello [c], Maria Vittoria Podda [b], Gaetano Paludetti [c], Massimiliano Papi [a], Alessandro Maiorana [a], Valentina Palmieri [a], Marco De Spirito [a], Anna Rita Fetoni [c]

[a] Istituto di Fisica, Università Cattolica (UCSC), Roma, Italy
[b] Istituto di Fisiologia, Università Cattolica (UCSC), Roma, Italy
[c] Dipartimento di Scienze Chirurgiche per le patologie della testa e del collo, Università Cattolica (UCSC), Roma, Italy

ARTICLE INFO

Article history:
Received 21 January 2014
Received in revised form 25 March 2014
Accepted 7 April 2014
Available online 13 April 2014

Keywords:
Reactive oxygen species (ROS)
Organ of Corti
Acoustic trauma
Two-photon microscopy
Laurdan
Lipid peroxidation

ABSTRACT

Background: Noise exposure impairs outer hair cells (OHCs). The common basis for OHC dysfunction and loss by acoustic over-stimulation is represented by reactive oxygen species (ROS) overload that may affect the membrane structural organization through generation of lipid peroxidation.
Methods: Here we investigated in OHC different functional zones the mechanisms linking metabolic functional state (NAD(P)H intracellular distribution) to the generation of lipid peroxides and to the physical state of membranes by two photon fluorescence microscopy.
Results: In OHCs of control animals, a more oxidized NAD(P)H redox state is associated to a less fluid plasma membrane structure. Acoustic trauma induces a topologically differentiated NAD(P)H oxidation in OHC rows, which is damped between 1 and 6 h. Peroxidation occurs after ~4 h from noise insult, while ROS are produced in the first 0.2 h and damage cells for a period of time after noise exposure has ended (~7.5 h) when a decrease of fluidity of OHC plasma membrane occurs. OHCs belonging to inner rows, characterized by a lower metabolic activity with respect to other rows, show less severe metabolic impairment.
Conclusions: Our data indicate that plasma membrane fluidity is related to NAD(P)H redox state and lipid peroxidation in hair cells.
General Significance: Our results could pave the way for therapeutic intervention targeting the onset of redox umbalance.

1. Introduction

The plasma membrane is vital to numerous cell functions including diffusion, energy generation, cell division, maintenance of electrochemical gradients and also provides a fluid matrix for embedded proteins essential to proper cell function [1,2]. Proteins and lipid–protein interactions contribute to membrane structure and modulate membrane fluidity [3]. Furthermore, the plasma membrane of cells is organized in many distinct microdomains with different lipid and protein compositions that appear to be associated with specific functional properties [4]. The organization of the plasma membrane in lipid domains affects its mechanical properties and the way it interacts with the underlying membrane skeleton [5]. This aspect is critically important in a specific cellular type, the cylindrical outer hair cells (OHCs) of the organ of Corti since, in these sensory cells, the characteristics of their plasma membrane are fundamental for the amplification of the level of sensitivity (up to 40–60 dB) and sharpened frequency selectivity of the hearing organ [6,7].

OHCs are polarized cells and lie in 3 rows (Fig. 1A). The OHC can be divided into apical, lateral and basal regions (Fig. 1C), each specialized for different functions [8,9]. Namely, the apical part, endowed with mechanosensitive ion channels [7], is responsible for the mechanism known as mechanoelectrical transduction (MET) whereas the lateral wall (LW) has a unique trilaminate structure composed of the plasma membrane, a subplasmalemmal cytoskeleton termed the cortical lattice, and a membranous organelle called the subsurface cisternae [10]. The membrane of the LW is also called somatic motor area in Fig. 1C, inasmuch houses dense clusters of voltage-sensitive plasma membrane-embedded motor elements identified as the protein prestin [11], that in turn modify the cell surface yielding the amplifying power (Fig. 1C) [12]. When exposed to intense acoustic noise, one of the major causes of hearing loss in adults in industrial societies [13], OHC's amplification and frequency discrimination results impaired [14]. The detrimental

Abbreviations: (NAD(P)H), Nicotinamide adenine dinucleotide phosphate; (ROS), Reactive oxygen species; (OHCs), outer hair cells; (MET), mechanoelectrical transduction; (LW), lateral wall; (ABR), auditory brainstem response; (4-HNE), 4-hydroxy-2-nonenal; (BSA), bovine serum albumin; (DMEM), Dulbecco's Modified Eagle's Medium; (GP), Generalized polarization; (ROI), Region of Interest

* Corresponding author at: Istituto di Fisiologia, Università Cattolica (UCSC), L.go Francesco Vito 1, 00168 Roma, Italy. Tel.: +39 0630154966.
E-mail address: d.troiani@rm.unicatt.it (D. Troiani).

http://dx.doi.org/10.1016/j.bbagen.2014.04.005
0304-4165/

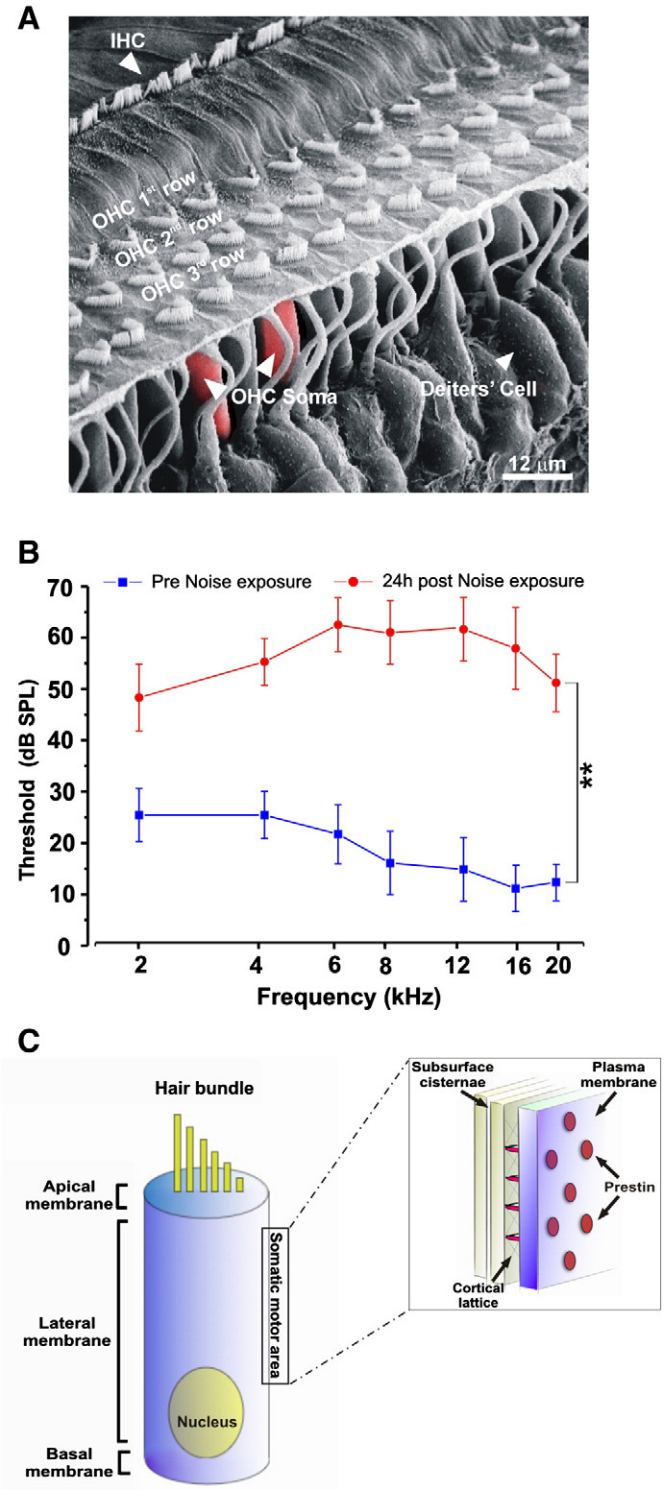

Fig. 1. Organization of the mammalian organ of Corti and hair cells on the basilar membrane and auditory functional evaluation (ABR). (A) Scanning Electron Microscopy (SEM) image of a cochlear basal turn showing the arrangement of hair bundles protruding beyond the reticular lamina in a view from above: IHC single row and OHC three rows; OHCs, in place over the basilar membrane are in series with Deiters' cells. SEM image is provided by A.R. Fetoni and S.L.M. Eramo. (B) Average auditory threshold ± SD before and at 24 h from noise exposure (n = 10 animals). Asterisks indicate significant effects; $^{**}p < 0.001$. (C) Schematic representation of the amplification process in OHCs. Both IHCs and OHCs are stimulated by a shear force applied to the stereocilia through the tectorial membrane. Following mechano-electrical transduction (MET), changes in the OHC membrane potential (*Vm*) act through the motor proteins and produce a longitudinal force in the cell to yield amplification and frequency selectivity. Inset in C illustrates the trilaminate structure of the Lateral Wall.

effects of noise appear concentrated in the organ of Corti, dominated by OHC loss and may involve also the *stria vascularis* and spiral ganglion neurons [14–16]. The currently accepted mechanism suggests that noise damage in the organ of Corti is triggered by mitochondrial reactive oxygen species (ROS) overproduction [17] which creates a self amplifying signaling loop under the participation of a number of enzymes [14,16,18]. Under normal conditions, the activation of this loop is limited by the antioxidant capacity of the cell and, among the redox regulation mechanisms, a crucial role is played by the reductive power provided by nicotinamide adenine dinucleotides (NAD) [19]. Whereas NADH mediates energy metabolism and mitochondrial functions, nicotinamide adenine dinucleotide phosphate, NAD(P)H, is a key component in cellular antioxidation systems [20]. However, mitochondrial ROS generation might not be overcome by NAD(P)H reducing power and ROS induced damage occurs. There is, in fact, substantial evidence that increased ROS production can lead to lipid peroxidation which disturbs the asymmetry of membrane lipids and may cause major changes in membrane characteristics including changes in fluidity [21]. Optimal fluidity is critical to OHC's shape and function [22]. Therefore, it is reasonable that modifications of the plasma membrane in terms of lipidic components and of their thermodynamic phases, as those induced by ROS, can have a crucial role in regulating OHC function [23,24]. However, mechanisms linking local redox variations in OHCs in their different functional zones and their effect on the physical state of membranes are still poorly understood. In addition, the time evolution of damage onset and the characterization of the oxidative process need further insights. Thus, to address these issues, we focused our research on the role played by NAD(P)H and on lipid peroxidation effects on the cytoplasmic membrane state.

We focused our study on the hair cells from the mid-high frequency regions (middle/basal turn OHCs) of the cochlea considering their higher susceptibility to the acoustic trauma with respect to the low frequency apical turn regions [6] and to other noise/ROS-affected cell types in the *stria vascularis* and in the spiral ganglion [17]. Specifically we investigated in the OHC distinct functional regions: a) the role of NAD(P)H by analyzing its spatial distribution and time evolution of its oxidation following noise exposure, b) the generation of lipid hydroperoxides, following the metabolic impairment, c) the organization of the plasma membrane by analyzing its fluidity through Laurdan two-photon microscopy.

2. Materials and methods

2.1. Animals

Adult Hartley albino guinea-pigs (age 3 months), weighing 250–300 g, with normal Preyer's reflex, were used in this study. All procedures regarding animal use, handling and care were conducted in accordance with the Laboratory of Animal Care and Use Committee of the Catholic University, School of Medicine of Rome, and of the European Communities Council Directive (86/609/EEC) and were approved by the Italian Department of Health (*Ministero della Salute*). The experiments were performed on 72 animals: 17 were used as controls and 55 were exposed to noise (of the latter, 25 were used for functional and oxidative damage analyses; the remaining 30 were functionally analyzed at different time points and then used for NAD(P)H and Laurdan two-photon microscopy).

2.2. Noise exposure

One day prior to the experiment, animals were mildly anesthetized with Ketamine hydrochloride 12.5 mg/kg, xylazine 2.5 mg/kg and acepromazine maleate 0.75 mg/kg body weight. Auditory function was assessed by recording auditory brainstem response (ABR) at low (2, 4 kHz), mid (6, 12 kHz) and high (16, 20 kHz) frequencies. ABR recordings were performed as reported in detail in previous papers [25,26]. Baseline ABRs were within the normal hearing range in all animals (Fig. 1B). On the day of the experiment, the acoustic trauma was

induced by a continuous pure tone of 6 kHz as described in previous papers [25,26]. A total of 55 guinea-pigs were exposed to acoustic trauma and sacrificed at different time points according to the different experimental procedures used in the present research. The animals were deeply anesthetized (Ketamine hydrochloride 25 mg/kg, xylazine 5 mg/kg and acepromazine maleate 1.5 mg/kg body weight), placed in a sound-proof room and exposed for 60 min to a 120 dB SPL pure tone sound at a frequency of 6 kHz. The sound was generated by a waveform generator (LAG-120B, Audio Generator, Leader Electronics Corporation, Yokohama, Japan), amplified by an audio amplifier (A-307R, Pioneer Electronics, Long Beach, CA, USA) and symmetrically presented in open field by a dome tweeter (TW340X0, Audax, Chateau du Loir, France) positioned 10 cm in front of the animal's head. Sound level was measured using a calibrated 1/4 in. microphone (Model 7017, ACO Pacific Inc., Belmont, CA, USA) and a calibrated preamplifier (Acoustic Interface System, ACO Pacific Inc). ABRs were recorded before and after the noise exposure at different time points (1, 3, 6, 9, 18 and 24 h) to control for the hearing impairment induced by the noise paradigm before processing the animals for the immunohistochemical analyses and NAD(P)H and membrane fluidity examinations. ABRs consistently produced an average threshold elevation of 40 dB (Fig. 1B). Consistent with previous data [18,25,26], the greatest hearing loss occurred in the 6–12 kHz region centered around the frequency of acoustic trauma.

2.3. Oxidative damage analysis in the cochlea

To assess lipid peroxidation induced by noise exposure we used 4-hydroxy-2-nonenal (4-HNE) immunostaining at 1, 6, 9, 18 and 24 h after acoustic trauma [16,18]. The analysis was performed in 25 noise exposed (10 cochleae/time point) and 5 control animals (10 cochleae). After the final ABR tests, animals were deeply anesthetized and sacrificed; the cochleae were quickly removed, and the samples were fixed with 10% buffered formalin in PBS at 4 °C a pH 7.5 for 24 h. The cochleae were then dissected in 0.1 M PBS and incubated in a blocking solution containing 1% fatty acid-free bovine serum albumin (BSA), 0.5% Triton X-100 and 10% rabbit serum in PBS for 2 h at room temperature [27]. The specimens were then incubated overnight at 4 °C with a solution containing rabbit polyclonal anti 4-HNE primary antibody (rabbit Anti 4-HNE antiserum, Cat#HNE11s, Alpha Diagnostics, TX, USA) diluted 1:100 in PBS. The rabbit anti-4HNE antibody cross-reacted with the guinea pig tissue. At the end of the incubation, all slides were washed twice in PBS and incubated at room temperature for 2 h, light-protected, in labeled conjugated goat anti-rabbit secondary antibody (Alexa Fluor 633, IgG, Invitrogen, Carlsbad, CA, USA) diluted 1:400 in 0.1 M PBS. After rinsing in PBS, the organs of Corti were mounted on slides and coverslipped with an antifade medium (ProLong Gold, Invitrogen). 4-hydroxynonenal positive cells were identified by red fluorescence scattered over the length of the organs of Corti. The images of 4-HNE immuno-labeled (40×–100×) were taken by a confocal laser scanning microscope (Leica Microsystem, Germany) equipped with an He/Ne laser (excitation 633 nm, emission 650–730 nm). Negative control experiments were performed by omitting the primary antibody during processing of tissue randomly selected across experimental groups (data not shown). Tissues from all groups were always processed together during the procedures to limit variability related to antibody penetration, incubation time and condition of tissue.

2.4. Organ of Corti preparation

All experiments were performed using freshly-dissected adult cochleae (60 cochleae from 30 noise exposed guinea pigs and 24 cochleae from 12 control animals). The deeply anesthetized animals were decapitated after auditory functional assessment at the different time points and the cochleae were rapidly removed. The temporal bones were taken and the middle ear bullae opened. The cochlear dissection was performed at room temperature (22–24 °C) in oxygenated artificial perilymph consisting of the following chemicals (mM): 5.4 KCl, 0.5 $MgCl_2$, 0.4 $MgSO_4$, 142 NaCl, 1.6 $CaCl_2$, 10.0 HEPES, 3.4 L-glutamine and 6.3 D-glucose. The pH of the solution was 7.4 (adjusted using NaOH) and osmolarity 300 mOsmol/l [28]. Thus the coiled organ of Corti was isolated, Reissner's membrane and *stria vascularis* were rapidly removed, the middle/basal, high-frequency (70–80% of basilar membrane length) region [16], highly susceptible to our noise paradigm [16,18], was selected and put in the oxygenated perilymph like HEPES-buffered solution. The pieces were, afterwards, immobilized on glass coverslips with antifade medium and analyzed for NAD(P)H microscopy (the right specimens) and prepared for Laurdan microscopy (the left specimens). In this preparation, the organ of Corti was structurally intact and the sensory cells retained a normal appearance (i.e. a uniformly cylindrical shape without regional swelling and a basally located nucleus) for up to 2 h after isolation of the cochlea.

2.5. NAD(P)H two photon microscopy

NAD(P)H is an intrinsically fluorescent molecule which may be excited by two photons of near infra-red (NIR) light. Since the NAD(P)H oxidized form $NAD(P)^+$ is not fluorescent, NAD(P)H redox state can be determined [29]. NAD(P)H fluorescence depends from the total molecule concentration $c = [NAD(P)^+] + [NAD(P)H]$, and this dependence can be modelized linearly, when quenching effect are neglected, by equation $F \sim c\varphi$, where $\varphi = [NAD(P)H]/c$ is the fraction of reduced pyridine nucleotide. Fluorescence monitors therefore both its redox balance (φ) and its anabolic/catabolic balance (c). c is changed by pyridine nucleotide depletion, due to nucleotide damage or NAD^+ consuming enzymes located in mitochondria (glycohydrolases), in the nucleus (PARP, sirtuins) and in Golgi complex (tankyrase) [19]. Molecule oxidation state, instead, will change φ. However, considering the usual range of variations of c (0.1 mM–2 mM) and φ (0.001, 0.1) [19], we can conclude that the contribution of c variations to F is negligible: the relative sensibilities of the technique toward these two variables are $\sigma_c = (\partial F/\partial c)_{\varphi\,=\,cost} = \varphi_0$, $\sigma_\varphi = (\partial F/\partial c)_{c\,=\,cost} = c_0$, and therefore $F = \sigma_\varphi \Delta\varphi + \sigma_c \Delta c$. Since in physiological conditions φ_0 is 1/700 (in mitochondria, where the most of autofluorescence arises from) and $c_0 \sim 1$ mM, NAD(P)H concentration variation in its whole range ($\Delta c \sim 1$ mM) gives a fluorescence contribution of $\sigma_c \Delta c = 1/700$ mM–0.001 mM. This is the same contribution given to F by a redox state variation $\Delta\varphi \sim 0.001$, which spans only 1/100 of its whole range. A decrease in c_0 and φ_0, approaching non-physiological states, could raise the contribution due to anabolic/catabolic unbalance, but when this difference becomes critical ($c_0 \sim \varphi_0$), F is under the limit of detection (0.1 mM) [30].

NAD(P)H intensity images were obtained with an inverted confocal microscope (DMIRE2, Leica Microsystems) using a 63× oil immersion objective (NA 1.4) under excitation at 760 nm with a mode-locked Titanium-Sapphire laser (Chameleon, Coherent, Santa Clara, CA). Internal photon multiplier tubes collected images in an eight bit, unsigned images at a 400 Hz scan speed. Intensity images were recorded with emission in the range of 400–500 nm and imaging was performed at room temperature. Successive focal planes were imaged in 2.5 μm steps for a total depth of 55–60 μm more than sufficient to encompass the entire depth of OHCs of the middle/basal turn. The interval between planes was chosen for optimum reconstruction of the cell volume without gaps. Images of 512 × 512 pixels were acquired at approximately 4/s with a pixel dwell time of 1.6 μs. Four scans were acquired and averaged to produce a single image. The analysis was performed on 30 animals at several time points from noise exposure (i.e., 1, 3, 6, 9, 18 and 24 h; n = 5 right specimens × time point). Data were compared with those obtained from control unexposed animals (n = 12). For each specimen, n = 80 cells were examined.

2.6. Laurdan two photon microscopy

Laurdan, 2-dimethylamino(6-lauroyl)naphthalene (Laurdan, Molecular Probes, Inc., Eugene, OR, USA), is a fluorescent dye highly sensitive to the presence and mobility of water molecules within the membrane bilayer, yielding information on membrane fluidity by a shift in its emission spectrum [31,32]. Fluidity is a broad term adopted to monitor the membrane state, which depends on the membrane structure, curvature, microviscosity as well as its phase, the lipid shape, packing and composition [3]. Laurdan exhibits an emission spectral shift depending on the lipid phase state, i.e. bluish in ordered, gel phases and greenish in disordered, liquid-crystalline phases. Laurdan distributes equally between lipid phases and does not associate preferentially with specific fatty acids or phospholipid headgroups [31]. The stock Laurdan (Molecular Probes, Inc., Eugene, OR, USA) solution concentration was 1 mM in dimethyl sulfoxide (DMSO; Sigma, St. Louis, MO) and it was renewed every three weeks [31,32]. 10 μl of Laurdan stock solution was added per milliliter of Dulbecco's Modified Eagle's Medium (DMEM). Laurdan labeling was performed directly on the excised freshly prepared specimens that were placed in a 5% CO_2 incubator for 30 min in the dark. Afterwards, the cover glass was washed once with DMEM and mounted upon a microscope slide. Laurdan intensity images were obtained with an inverted confocal microscope (DMIRE2, Leica Microsystems, Germany) using a 63× oil immersion objective (NA 1.4) under excitation at 800 nm with a mode-locked Titanium-Sapphire laser (Chamaleon, Coherent, Santa Clara, CA). Internal photon multiplier tubes collected images in an eight bit, unsigned images at a 400 Hz scan speed. Laurdan intensity images were recorded simultaneously with emission in the range of 400–460 nm and 470–530 nm and imaging was performed at room temperature. The analysis was performed on 30 animals at several time points from noise exposure (1, 3, 6, 9, 18 and 24 h); (n = 5 left cochlear specimens × time point). Data were compared with those obtained from control unexposed animals (n = 12). For each specimen, n = 80 cells were examined.

2.7. NAD(P)H and 4-HNE fluorescence images

Background values of NAD(P)H and 4-HNE fluorescence images (defined as intensities below 7% of the maximum intensity) were set to zero in ImageJ. NAD(P)H fluorescence values were recovered from fluorescent images, and averaged over multiple regions of interest. PMT and excitation intensity were not changed in the measurement session.

2.8. Generalized polarization images (GP)

As a normalized ratio of the intensity at the two emission wavelengths regions, the generalized polarization (GP) provides a measure of membrane order, in the range between −1 (liquid-crystalline) and +1 (gel). The GP, defined as

$$GP = \frac{I_{(400-460)} - GI_{(470-530)}}{I_{(400-460)} + GI_{470-530}} \quad (1)$$

was calculated for each pixel using the two Laurdan intensity images ($I_{(400–460)}$ and $I_{(470–530)}$) by using the program Ratiometric Image processor [33]. The calibration factor G was obtained from the GP values of solutions of Laurdan in DMSO. G factor had ~2% variation across the imaging area. GP images (as eight-bit unsigned images) were pseudocolored in ImageJ. Background values (defined as intensities below 7% of the maximum intensity) were set to zero.

GP values for PM membranes were determined within multiple Regions of Interest for each sample (free hand ROIs draw on cell membranes: an example is shown in Fig. 2B in red and indicated by an arrow) [34]. Traced Regions of Interest (ROIs) were characterized by a length of several microns, and by a pixel resolution width. Values for plasma membranes were determined within multiple ROIs (annulus ROIs on cell membranes). For each sample n = 80 OHCs per specimen were analyzed [34]. Line profiles and analysis of acquired images were performed with ImageJ.

2.9. Statistical analyses

ABR data are presented as Mean ± SD and differences were assessed by using the analysis of variance (ANOVAs with repeated measures), followed by Tukey's multiple comparison test (Statistica Statsoft, Tulsa, OK, USA); values of $p < 0.05$ were considered significant. For NAD(P)H intensities and GP data, Mean ± SD values were determined and utilized for two-tailed Student's *t*-test analysis.

3. Results

3.1. Spatial organization of NAD(P)H in OHCs

NAD(P)H imaging of the middle/basal turn of excised preparations of Corti's organ showed that NAD(P)H fluorescence levels in all cell types stayed stable (within error) over the course of 60 min (Fig. 1 electronic supplementary materials). In Fig. 2A, NAD(P)H intensity images are reported versus the distance from the basal part of the cell (see Fig. 1C), in a pseudo-colored green scale. Mean NAD(P)H fluorescence values of inner row OHCs, are reported in Fig. 2C against the distance from the basal part of the cell. The curve is bell-shaped, peaked in the middle of the cell, and with minimum values at apical and basal regions. The bell-shaped curve reflects an heterogeneity in the reduced NAD(P)H concentration in the cell [29]. Reduction of the redox couple is therefore mainly localized in the region of the LW, and oxidation at apical and basal regions. The lower part of the cell body, in the region of plasma membrane, is characterized by an higher oxidation with respect to the hair bundle region (~40% more oxidized, Fig. 2C). Z-profiles of middle and outer rows have similar shapes, as shown in Fig. 3B and C (full squares), although NAD(P)H redox state is different among rows, increasing its value from the inner to the outer row (Fig. 3A-C): in the middle row is 8% higher, whereas in the outer row is 26% higher, suggesting that different rows are characterized by distinct metabolic activities.

3.2. Generalized polarization (GP) of plasma membrane in OHC cells

In Fig. 2B, ratiometric Laurdan fluidity maps of OHCs are reported versus distance from the basal part of the cell in a pseudo-colored rainbow scale, spanning from blue (very fluid) to red (very rigid) through green (intermediate fluidity). From the maps high GP values are evident for the hair bundle (85% of cell length, Fig. 2B). Membranes are generally less fluid than inner organelles in the cells (30% of cell length, Fig. 2B) as expected [31,32]. By analyzing specifically the plasma membrane GP values (Fig. 2C) against the distance from the basal part of the cell, we observed a valley-shaped, curve with a minimum in the middle region of the cell (LW) and two maxima in correspondence of cell extremities (hair bundle and basal part, see Fig. 1A,C). Plasma membranes in the stereocilia region show a GP value of 0.53, which decreases consistently when moving toward the basal region of the cell. The plasma membrane in the lower part of the cell body has a lower GP value (0.47). This GP modulation reflects a different structural composition of the plasma membrane in the hair bundle region and in the cell body region, due to their different structural and functional roles. No differences of GP values distribution were detected among OHC rows.

3.3. Spatial anti-correlation between NAD(P)H and GP values

As reported in Fig. 2D, where GP values are plotted versus NAD(P)H values, an evident negative correlation is observed that can be described by a simple equation:

$$GP = GP_{ox} - m[NAD(P)H] \quad (2)$$

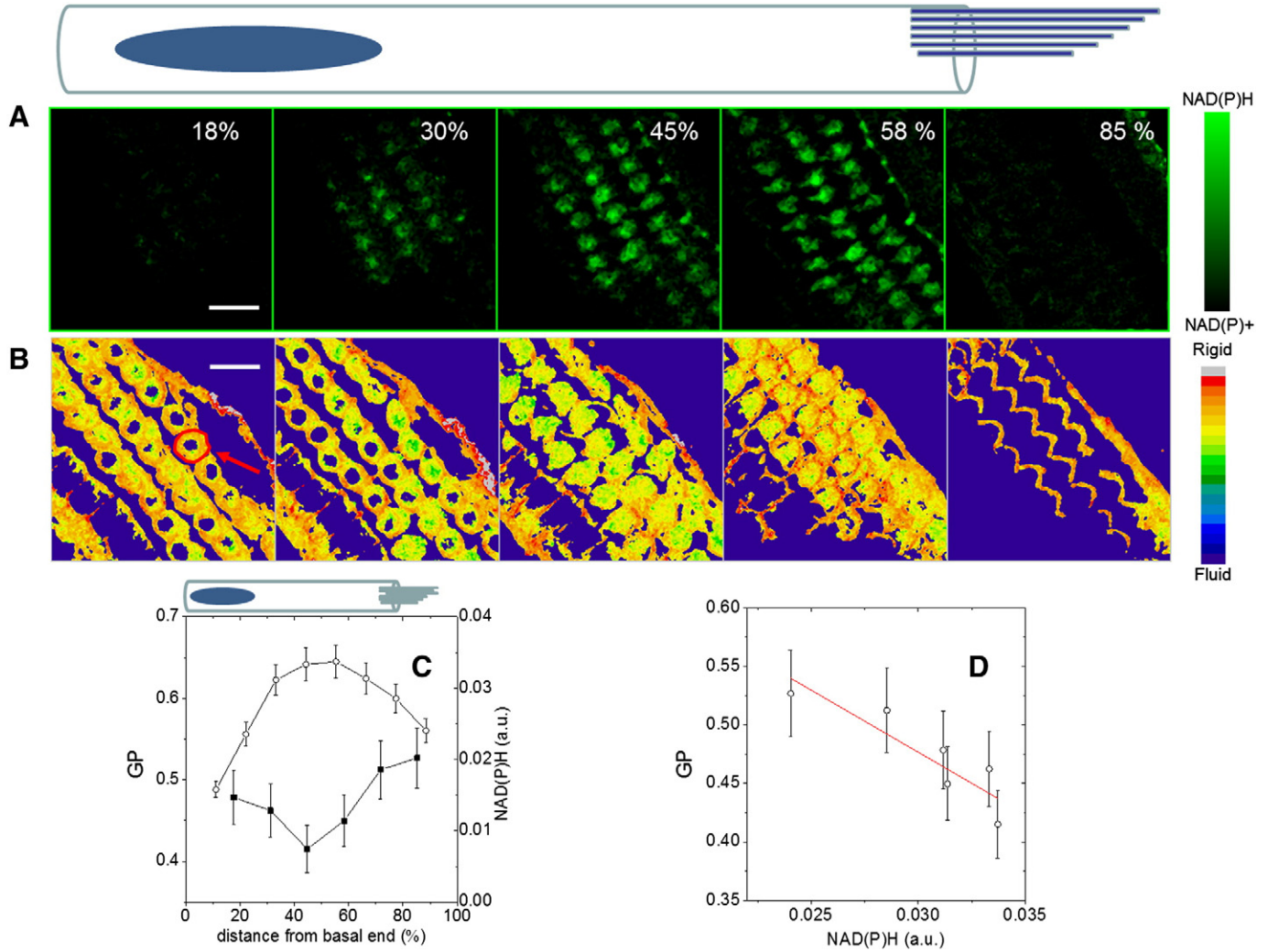

Fig. 2. Spatial organization of NAD(P)H and fluidity in OHCs. (A) NAD(P)H intensity images versus the distance from the basal part of the cell, reported in a pseudo-colored green scale. (B) Ratiometric Laurdan fluidity maps are reported versus the distance from the basal part of the cell, in a pseudo-colored rainbow scale, spanning from blue (very fluid) to red (very rigid) through green (intermediate fluidity). (C) Mean NAD(P)H fluorescence values (open circles) (n = 80 cell from the right specimens of 5 animals at each time point) and mean GP values (closed circles) (n = 80 cell from the left specimens of 5 animals at each time point) are reported against the section height, from the hair bundle to the cell body region. (D) Axial anti-correlation between NAD(P)H and GP values. Values are fitted according to the equation $GP = GP_{ox} - m[NAD(P)H]$ where $GP_{ox} = 0.78$ is the GP value when all [NAD(P)H] is in its fully oxidized form, and $m = -10.1$ is the slope (in auxiliary units). Solid line is the fit to the data.

where GP_{ox} is the GP value when all [NAD(P)H] is in its fully oxidized form, and m is the slope (in auxiliary units). A fit of this equation to the experimental data allows to recover $GP_{ox} = 0.79$, and $m_x = -10.2$.

3.4. Acoustic trauma induces a topologically differentiated NAD(P)H oxidation on OHCs

We analyzed the effect of acoustic trauma on the NAD(P)H distribution of inner, middle and outer rows of OHCs in the noise-affected middle/basal turn of the cochlea. In Fig. 3A we report mean NAD(P)H fluorescence values of the inner row of OHCs against distance from the basal part of the cell. The bell-shaped curves, 1 h after the trauma, show a 30% decrease of NAD(P)H fluorescence for almost every value along the whole length of the cell. At 3 h and 6 h after the trauma the overall fluorescence shows further little decrease. On the contrary, 9 h after trauma the NAD(P)H signal shows a stronger decrease (overall loss: ~70%). At 18 h and at 24 h the signal is absent.

In Fig. 3B and in Fig. 3C mean NAD(P)H fluorescence values are reported respectively for the middle and outer OHC rows against the distance from the basal part of the cell. Control fluorescence at t = 0 (absence of any acoustic stress) of the outer row is higher than that of the middle row, which in turn is higher than that of the inner row. Furthermore, at the time point 1 h after noise exposure, the decrease of fluorescence of the outer row, is higher than that of the middle row, which in turn is higher than that of the inner row. From 3 h till 24 h, the behavior is similar among rows.

Representative fluorescence NAD(P)H images at different time points (0 h, 1 h, 6 h, 9 h, 18 h) after the trauma are reported in Fig. 4A. The graph in Fig. 4D reports the corresponding reduced NAD(P)H percentages. Fig. 4D shows the topologically differentiated NAD(P)H oxidation on the outer, middle and inner rows of OHCs. NAD(P)H oxidation is highly non linear. In each of the three rows, a fast drop off of the fluorescence signal is followed by a plateau between 1 h and 6 h after the trauma, when the signal stays nearly constant. At this time interval, NAD(P)H concentration is more damped in inner rows with respect to outer rows: in the inner rows ~65% of NAD(P)H reservoir is still present, whether in the middle and in the outer rows the percentage is respectively ~50% and ~45%. Afterwards, the NAD(P)H decreases till the exhaustion of the reduced milieu. In Fig. 5A, magnified particulars of NAD(P)H fluorescence at the time points 0 h and 9 h show how the main contribution come from mitochondria, as observed elsewhere [29].

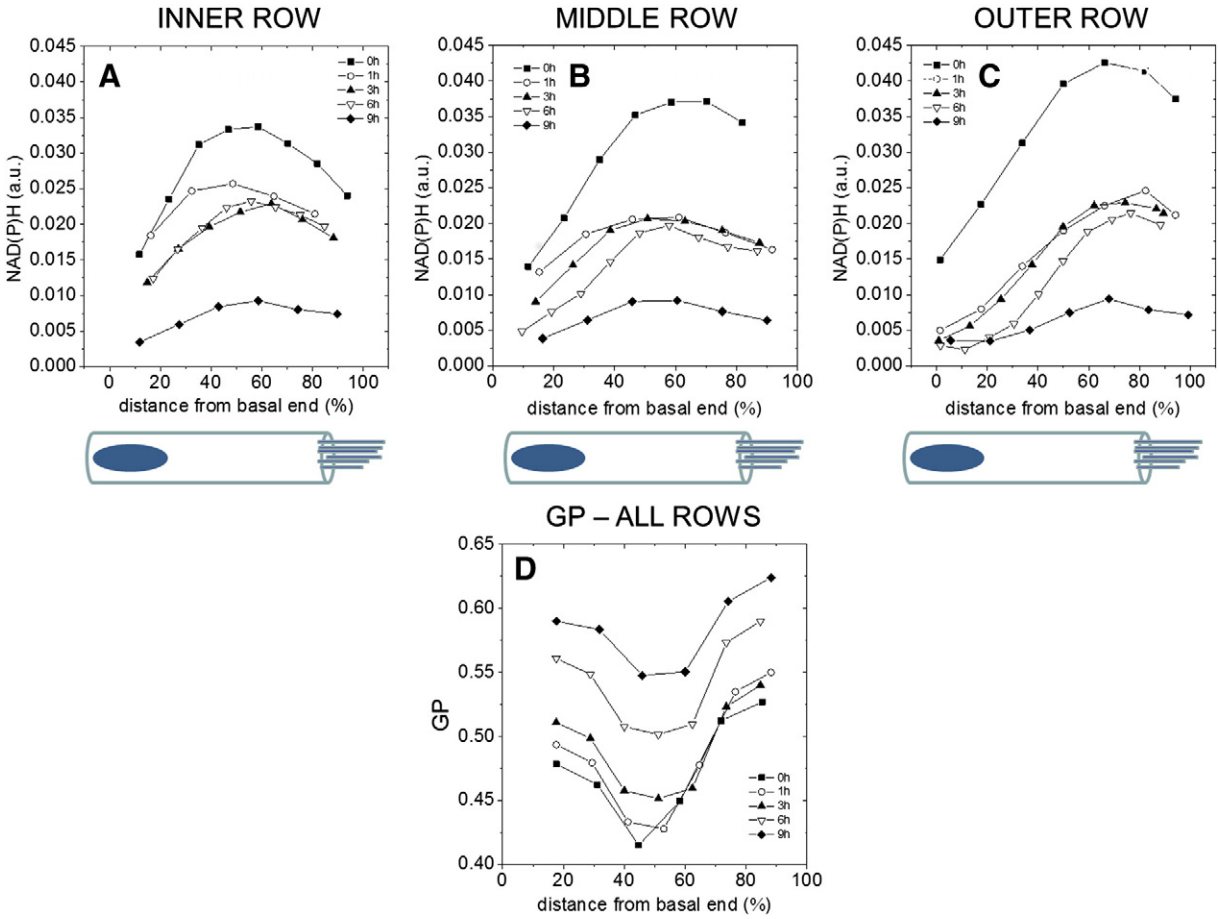

Fig. 3. Acoustic trauma induces topologically differentiated NAD(P)H oxidation and fluidity loss of plasma membrane. (A) Mean NAD(P)H fluorescence values of the inner row of OHCs versus distance from the basal part of the cell. (B) Mean NAD(P)H fluorescence values of the middle row of OHCs versus distance from the basal part of the cell. (C) Mean NAD(P)H fluorescence values of the outer row of OHCs, versus distance from the basal part of the hair cell. Control NAD(P)H fluorescence is about 25% higher with respect to the inner row cells. (D) Mean GP values of the outer row of OHCs, versus distance from the basal part of the cell.

3.5. Acoustic trauma induces lipid peroxidation

It is well known that lipid oxidation is a common hallmark of oxidative stress. Among the biomarkers of lipid peroxidation, 4-HNE is one of the most sensitive and widely used in several in vitro and in vivo experimental systems. A faint staining was observed in control animals (Fig. 4B). As shown in Fig. 4B, the organ of Corti from noise exposed guinea-pigs underwent oxidative stress. A strong immunoreactivity for 4-HNE was detected in almost all OHCs, in the severely damaged area located in the middle/basal turn of the cochlea. 4-HNE immunostaining progressively increased from 1 to 9 h. At 18 h after noise exposure 4-HNE remained strongly expressed, with no further increase, as compared to 9 h. At 24 h, a slight increase was observed as compared to the previous time point (data not shown). The graph in Fig. 4E reports the corresponding 4-HNE percentages images at different time points (0 h, 1 h, 6 h, 9 h, and 18 h) after the trauma. In Fig. 5B, magnified particulars of 4-HNE fluorescence at the time points 0 h and 9 h show how the contributions comes mainly from plasma membranes.

3.6. Acoustic trauma induces an increase of GP in OHC plasma membrane

In Fig. 3D mean plasma membrane GP values are reported for the outer row of OHCs, against the distance from the basal part of the cell, as there were no significant differences of GP values distribution among rows (data not shown). At all times after the trauma, the characteristic asymmetric shape is retained. One h after the trauma, the GP profile remains almost identical with respect to the control, except for the maximum GP value in the hair bundle region, which increases ($\Delta GP \approx 0.5$), indicating that the hair bundle membranes undergo a structural modification (fluidity loss). Three hours after the trauma, the overall GP profile shifts to higher values. Nine hours after the trauma, the GP value of the hair bundle again increases and an evident fluidity loss at others z sections occurs. A further fluidity loss is present at 18 h, where also the difference between extreme GP values is reduced. Therefore, the acoustic trauma induces fluidity loss of OHC plasma membrane (more evident at 18 h, 24 h time points in the hair bundle region). Fig. 4C illustrates the fluidity maps at different time points after the acoustic trauma. In Fig. 4F the GP values of the hair bundle (maximum of the GP profiles) are reported. The GP values stay nearly constant for 6 h before starting to increase.

In Fig. 5C, magnified particulars of GP values show how 9 h after noise exposure cell membranes become less fluid (more red) compared to control (0 h).

4. Discussion

To address the effect of redox homeostasis on plasma membrane fluidity in OHCs, responsible for amplification and frequency selectivity of hearing, we have investigated the intracellular NAD(P)H spatial distribution, the induction of lipid peroxidation and the related variations in plasma membrane fluidity in physiological and pathological conditions (i.e. after acoustic stress).

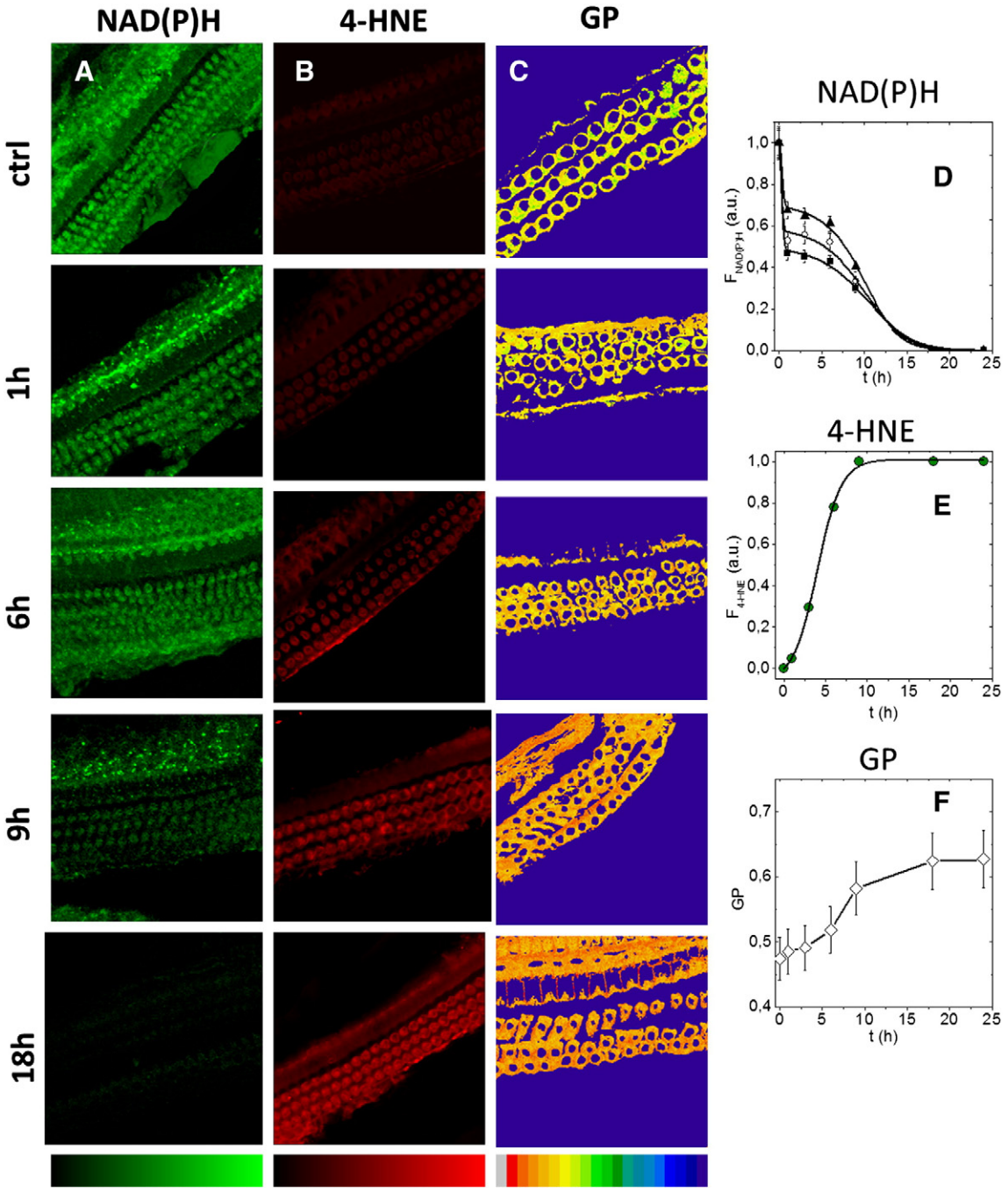

Fig. 4. Acoustic trauma induces NAD(P)H oxidation, lipid peroxidation and loss of membrane fluidity. (A) Representative fluorescence NAD(P)H images at different times points (n = 5 animals per time point) after the trauma. (B) 4-HNE assays at different times after acoustic trauma. (C) Fluidity maps at different times after acoustic trauma. (D) Reduced NAD(P)H percentages at different times after the trauma. From the figure it is also evident the topologically differentiated NAD(P)H oxidation on the outer, middle and inner rows of OHCs. (E) 4-HNE concentrations at different times after acoustic trauma. (F) GP values of hair bundle region (maximum of the GP profiles) at different times after the trauma.

4.1. Spatial distribution of noise induced oxidation and membrane fluidity changes

In physiological conditions the OHC lateral wall was fluid and NAD(P)H appeared reduced, while at the hair bundle region, and in the basal part of the cell, the plasma membrane was more rigid and NAD(P)H more oxidized. The observed linear anti-correlation between membrane structural state, as revealed by GP value and NAD(P)H spatial distribution, suggests a functional linkage between the two parameters. This observation suggests that the different regions have dissimilar structural membrane composition and metabolic state likely related to their specialized role in OHC function. Indeed, the amplification process is triggered by sequential mechanisms: the active hair bundle motion through the mechanosensitive MET channels [7,35], which induce a modification of cell's membrane potential leading to active force production arising from the voltage-sensitive motor protein prestin [6,36]. These two mechanisms are in turn controlled by the membrane structural organization and regional differences of lipid components are reported in OHC plasma membrane concerning, specifically, the crucial component cholesterol [5,37]. Interestingly, previous studies using fluorescent labels suggest that cholesterol concentration in the OHC lateral wall is significantly lower than in the apical or basal

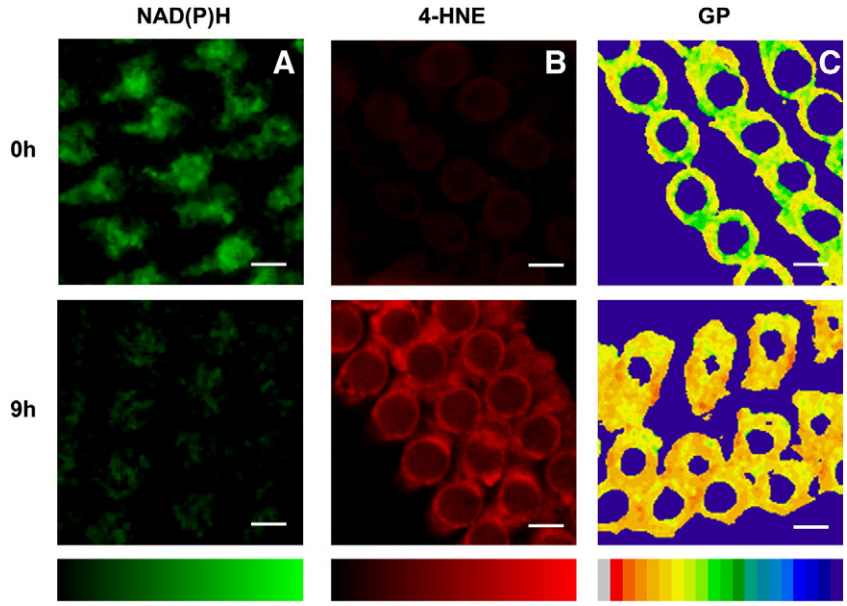

Fig. 5. Spatial localization of NAD(P)H oxidation, lipid peroxidation and loss of membrane fluidity. (A) Magnified particulars of NAD(P)H fluorescence at the time points 0 h and 9 h showing how it arises mainly from mitochondria. (B) Magnified particulars of 4-HNE fluorescence at the time points 0 h and 9 h showing how the contribution comes mainly from plasma membranes. (C) Magnified particulars of GP values at the time points 0 h and 9 h showing how high values are characteristics of cell membranes (red) which become gradually more red at longer time points after noise exposure. After the noise insult, OHC cells change their morphology, as shown by the slight increase of the cell area section.

regions [10,38]. The spatial distribution of GP we observed along the length of the OHC is consistent with the above mentioned difference in membrane cholesterol (LW: low concentration of cholesterol, low GP and fluid membrane; hair bundle: high cholesterol, high GP value and rigid membrane). Additionally, cholesterol was shown to influence prestin distribution, self-association, and the voltage dependence of prestin-associated charge movement [39]. Furthermore, there are data consistent with our GP values on the bell-shaped distribution of prestin-associated charge density along OHC lateral wall [40,41].

In pathological conditions, we observed a significant NAD(P)H oxidation, indicative of changes or dysfunction in OHC metabolism [24,42]. NAD(P)H provides the reducing equivalents for biosynthetic reactions and the oxidation-reduction involved in protecting against the toxicity of ROS, allowing the regeneration of reduced glutathione [19]. We found that NAD(P)H oxidation drop was followed by a rise of plasma membrane peroxidation (Fig. 4E) and an abrupt decrease of fluidity (Fig. 4F). The close correlation between the lipid peroxidation levels and the rigidity of cell membrane suggests a possible cause/effect relationship between the two phenomena. Nevertheless, further studies are needed to specifically assess and unravel the molecular pathway linking NAD(P)H oxidation and changes in OHC membrane fluidity. Howewer, numerous studies have reported decreases in membrane fluidity secondary to lipid peroxidation caused by oxidative damage [24,43]. This mechanism can lead to membrane destructuration and to modulation of the intermolecular interactions between the molecular motor prestin and lipids and/or the associated complex pattern of cytoskeletal elements and submembranous endoplasmic reticula [5,10]. Indeed, the underlying cytoskeleton meshwork (actin filaments, spectrin tetramers organized in microdomains) interacts with the plasma-membrane-embedded motor molecules [44] and ROS effects on cytoskeletal proteins (e.g. depolymerization of actin filaments) are plausible [45]. Hence, not only membrane lipid composition (e.g. cholesterol level known to affect microdomain dynamics in a region-dependent manner) but also membrane-cytoskeleton integrity may regulate the general dynamics of LW [12]. Thus a rearrangement of prestin tight packing [46] and a functional impairment of OHCs at the level of active force production phase (Fig. 6A) can be expected. Furthermore, considering that both lowering and raising the cholesterol levels result in alterations of membrane protein function [38,39,47] and that hypercholesterolemia may be linked to hearing loss both in animal models and humans [5], it is possible that the observed increase in GP could be due, at least in part, to the peroxidation induced alterations of cholesterol packing [43] and to cholesterol trafficking [48]. However, our Laurdan microscopy approach does not distinguish membrane fluidity from cholesterol-content changes but a direct association between these two parameters has been reported in cultured cells by using different techniques [49]. Further investigations are needed to specifically address this issue.

Finally, in noise exposed animals, the spatial distributions of NAD(P)H oxidation highlights distinct properties for OHCs belonging to different rows in facing the stress insult: OHCs belonging to inner rows, characterized by a lower metabolic activity, show a less severe metabolic impairment with respect to the other rows before the onset of membrane destructuration triggered by lipid peroxidation. A schematic representation of the noise induced membrane fluidity loss of OHC cells is reported in Fig. 6A.

4.2. Time course of noise induced NAD(P)H, 4-HNE and GP changes

Our data on the level of peroxidation, GP value and NAD(P)H oxidation, have shown that while the former two have a sigmoidal trend the latter parameter is highly non linear (Fig. 6B). Specifically, in each of the three rows, a fast drop off of oxidation is followed by a plateau between 1 h and 6 h after trauma, when the signal stays nearly constant. Afterwards, NAD(P)H decreases till exhaustion of the reduced milieu. The time course of the three parameters has been compared and, in order to determine the characteristic times of OHC damage induction, we modeled NAD(P)H drop off, peroxidation and fluidity with an empirical function constituted of a single exponential summed to a Boltzmann sigmoidal function.

As regards NAD(P)H drop off

$$F_{NAD(P)H} = A_{OX1} e^{-\frac{t}{\tau_{OX1}}} + \frac{A_{OX2}}{\left(1 + e^{\frac{t-\tau_{OX2}}{dt}}\right)} \tag{3}$$

where A_{ox1} and A_{ox2} are the amplitudes of the two functions, τ_{ox1} is the first decay time, τ_{ox2} is the second decay time and $\delta\tau_{ox}$ is the characteristic time scale of the sigmoid.

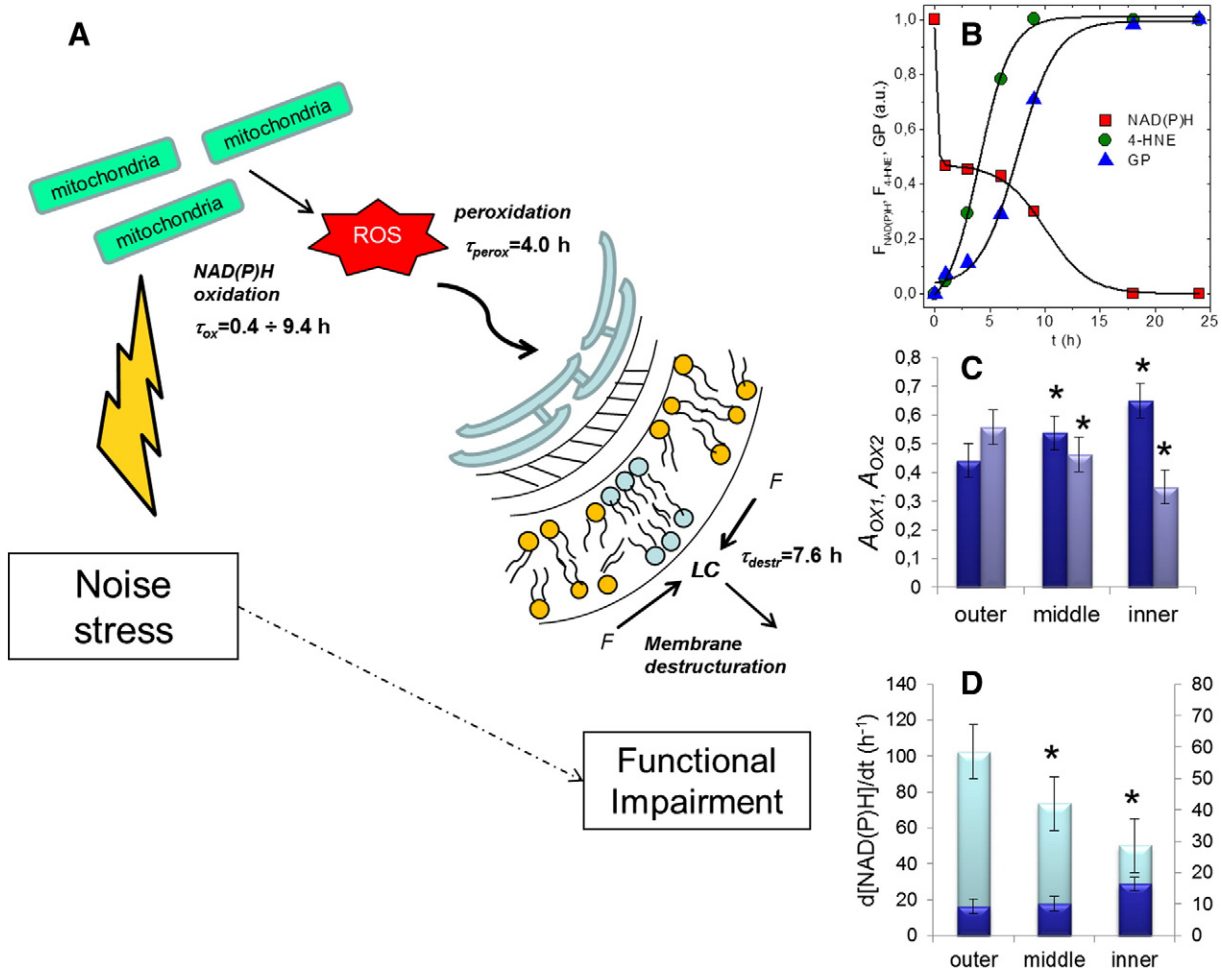

Fig. 6. Model of OHC's functional impairment. (A) Noise stress induces NAD(P)H drop, which is followed by free radical accumulation and a consequent rise of plasma membrane peroxidation. Peroxidation leads to a membrane destructuration consisting in a cytoplasmic membrane loss of fluidity. (B) Oxidation of NAD(P)H, 4-HNE peroxidation and GP increase. NAD(P)H oxidation is highly non linear. In each of the three rows, a fast drop off of oxidation is followed by a plateau between 1 h and 6 h after trauma, when the signal stays nearly constant. Afterwards, NAD(P)H decreases again till the exhaustion of the reduced milieu. 4-HNE peroxidation has a sigmoid trend, and advances the GP increase, which is also sigmoid. (C) Difference in control NAD(P)H redox state among rows quantified through A_1 (blue bar), A_2 (violet bar). Asterisks indicate significant effects; $^*p < 0.05$. (D) Rate of NAD(P)H exhaustion in the first (cyan bars) and in the second decay (blue bars), for each of the three rows. The inner rows show a slightly higher time resistance to oxidation in the first drop off, with a decay rate of 50% per hour with respect to the middle row (74% per hour) and the outer row (103% per hour). During the second decay, the rate of NAD(P)H exhaustion seems slightly higher going from the outer to the inner row. Asterisks indicate significant effects; $^*p < 0.05$.

The fit (Fig. 4D) reveals two characteristic oxidation times: a faster one (τ_{ox1} ~ 0.36 h) and a slower one (τ_{ox2} ~ 9.43 h).

While the faster and the slower oxidation times are invariant among rows, the plateau reached by the NAD(P)H redox state after the first decrease is different among rows, increasing its value from the outer to the inner row, as shown by the parameter A_{ox2} which increases from 50% to 70%, whereas the weight of the second exponential decreases accordingly (Fig. 6C). We determined the rate of NAD(P)H exhaustion in the first and in the second decay, for each of the three rows, throughout respectively the formulas $s_{fast} = -\frac{1}{\tau_1}\ln\left(A_{ox1} + \frac{A_{ox2}}{2}\right)$ and $s_{slow} = \frac{A_{ox2}}{4\delta\tau_{ox2}}$ (Fig. 6D). The inner rows show a slightly higher time resistance to oxidation in the first drop off, with a decay rate of 50% per hour, with respect to the middle row (74% per hour) and the outer row (103% per hour) (Fig. 6D). Contextually, the initial NAD(P)H redox state decreases going from the outer to the inner rows (Fig. 3A-C). During the second decay, the rate of NAD(P)H exhaustion is slightly higher going from the outer to the inner row. These differences are functional, because distinct metabolic states give to OHCs distinct properties in facing the stress insult: in inner rows, a lower metabolic activity is associated to a higher resistance in the first phases of noise stress.

The 4-HNE peroxidation has a sigmoidal trend, and advances the GP increase, which is also sigmoidal. Therefore, 4-HNE concentration increase can be modeled according to a Boltzmann sigmoidal function

$$F_{4HNE} = A_2 + \frac{A_1 - A_2}{\left(1 + e^{-\frac{t-\tau_{perox}}{\delta\tau_{perox}}}\right)} \tag{4}$$

where A_1 and A_2 are the baseline and the plateau of the sigmoid, τ_{perox} is the characteristic time of the peroxidation ($\tau_{perox} = 4.0$ h), and $\delta\tau_{perox}$ is the characteristic time scale of the sigmoid. Also GP increase can be modeled according to a Boltzmann sigmoidal function

$$GP = B_2 + \frac{(B_1 - B_2)}{\left(1 + e^{\frac{t-\tau_{destr}}{\delta t}}\right)} \tag{5}$$

where B_1 and B_2 are the baseline and the plateau of the sigmoid, and τ_{destr} is the characteristic time of the membrane destructuration ($\tau_{destr} = 7.6$ h), and $\delta\tau_{destr}$ is the characteristic time scale of the sigmoid.

On the whole, we found that NAD(P)H drop is characterized by a fast characteristic time (τ_{ox1} ~ 0.36 h), before reaching a steady state. OHCs belonging to inner rows, characterized by a lower metabolic activity, show the smallest variation of NAD(P)H reservoir suggesting a less severe metabolic impairment with respect to other rows. During this steady state, free radical accumulation leads to a consequent rise of plasma membrane peroxidation with a characteristic time $\tau_{perox} = 4.0$ h. This in turn leads to a membrane destructuration, with a characteristic time $\tau_{destr} = 7.6$ h. After the onset of membrane destructuration, triggered by lipid peroxidation, NAD(P)H decreases till exhaustion with a characteristic time τ_{ox2} ~ 9.4 h. These observations are of particular clinical interest since the development of an effective antioxidant intervention plan would increase the protection of OHC cells from cell death [14, 50]. A rescue effect could be obtained in the guinea pig model since we have shown how ROS are still damaging cells for a period of time after the noise exposure has ended (~7.5 h). Consistent with our findings, oxidative DNA damage is reported to begin 8 h after noise exposure [51]. Therefore in our model, the 7.5 h after noise exposure may be taken as an important time window for antioxidant rescuing intervention. Our results suggest that antioxidants could exert their best effect before the onset of the peroxidation reactions, which occur at a lower characteristic time ($\tau_{perox} = 4.0$ h).

In conclusion, we have presented data and a model that describes the mechanism by which oxidation modulates, through lipid peroxidation, the plasma membrane fluidity of OHCs. Membrane fluidity loss influences the micromechanics of the OHC lateral wall. While in control animals a functional relation is established between membrane fluidity and NAD(P)H distribution, in noise exposed animals membrane fluidity abruptly decreases as a consequence of excess peroxidation, induced by an alteration in the metabolic state. Additionally, the different capability of OHCs belonging to different rows to face the noise insult is strictly correlated to NAD(P)H distribution. Our findings thus, show: a) how membrane fluidity is related, both in physiological and pathological conditions, to NAD(P)H redox state and lipid peroxidation, which represent key targets for a therapeutic rescuing plan from noise insults and b) by considering the kinetics of damage onset, that the best therapeutic interventions should be implemented during the critical post-traumatic period.

Acknowledgements

This work was supported by Fondi di Ateneo, UCSC Rome, Italy. The confocal analysis has been performed at Labcemi, UCSC, Rome. The authors acknowledge the COST Action CM1201 “biomimetic radical chemistry” for useful discussions and express their gratitude to Dr Rolando Rolesi for figure preparation. The authors declare no conflicts of interest related to this work.

Appendix A. Supplementary data

Supplementary data to this article can be found online at http://dx.doi.org/10.1016/j.bbagen.2014.04.005.

References

[1] M. Edidin, Lipids on the frontier: a century of cell-membrane bilayers, Nat. Rev. Mol. Cell Biol. 4 (2003) 414–418.
[2] S. Sonnino, A. Prinetti, Membrane domains and the “lipid raft” concept, Curr. Med. Chem. 20 (2013) 4–21.
[3] G. Lenaz, Lipid fluidity and membrane protein dynamics, Biosci. Rep. 7 (1987) 823–837.
[4] D.M. Owen, A. Magenau, D. Williamson, K. Gaus, The lipid raft hypothesis revisited—new insights on raft composition and function from super-resolution fluorescence microscopy, Bioessays 34 (2012) 739–747.
[5] L.E. Organ, R.M. Raphael, Lipid lateral mobility in cochlear outer hair cells: regional differences and regulation by cholesterol, J. Assoc. Res. Otolaryngol. 10 (2009) 383–396.
[6] A.J. Hudspeth, Making an effort to listen: mechanical amplification in the ear, Neuron 59 (2008) 530–545.
[7] J. Ashmore, Cochlear outer hair cell motility, Physiol. Rev. 88 (2008) 173–210.
[8] W.E. Brownell, A.A. Spector, R.M. Raphael, A.S. Popel, Micro- and nanomechanics of the cochlear outer hair cell, Annu. Rev. Biomed. Eng. 3 (2001) 169–194.
[9] J. Santos-Sacchi, New tunes from Corti's organ: the outer hair cell boogie rules, Curr. Opin. Neurobiol. 13 (2003) 459–468.
[10] J.S. Oghalai, A.A. Patel, T. Nakagawa, W.E. Brownell, Fluorescence-imaged microdeformation of the outer hair cell lateral wall, J. Neurosci. 18 (1998) 48–58.
[11] J. Zheng, W. Shen, D.Z. He, K.B. Long, L.D. Madison, P. Dallos, Prestin is the motor protein of cochlear outer hair cells, Nature 405 (2000) 149–155.
[12] R. Kitani, C. Park, F. Kalinec, Microdomains shift and rotate in the lateral wall of cochlear outer hair cells, Biophys. J. 104 (2013) 8–18.
[13] M.D. Seidman, R.T. Standring, Noise and quality of life, Int. J. Environ. Res. Public Health 7 (2010) 3730–3738.
[14] D. Henderson, E.C. Bielefeld, K.C. Harris, B.H. Hu, The role of oxidative stress in noise-induced hearing loss, Ear Hear. 27 (2006) 1–19.
[15] Y. Wang, K. Hirose, M.C. Liberman, Dynamics of noise-induced cellular injury and repair in the mouse cochlea, J. Assoc. Res. Otolaryngol. 3 (2002) 248–268.
[16] A.R. Fetoni, P. De Bartolo, S.L.M. Eramo, R. Rolesi, F. Paciello, C. Bergamini, R. Fato, G. Paludetti, L. Petrosini, D. Troiani, Noise-induced hearing loss (NIHL) as a target of oxidative stress-mediated damage: cochlear and cortical responses after an increase in antioxidant defense, J. Neurosci. 33 (2013) 4011–4023.
[17] N. Raimundo, L. Song, T.E. Shutt, S.E. McKay, J. Cotney, M.X. Guan, T.C. Gilliland, D. Hohuan, J. Santos-Sacchi, G.S. Shadel, Mitochondrial stress engages E2F1 apoptotic signaling to cause deafness, Cell 148 (4) (2012) 716–726.
[18] A.R. Fetoni, C. Mancuso, S.L. Eramo, M. Ralli, R. Piacentini, E. Barone, G. Paludetti, D. Troiani, In vivo protective effect of ferulic acid against noise-induced hearing loss in the guinea-pig, Neuroscience 169 (2010) 1575–1588.
[19] W. Ying, NAD/NADH and NADP/NADPH in cellular functions and cell death: regulation and biological consequences, Antioxid. Redox Signal. 10 (2008) 179–206.
[20] G. Lenaz, M.L. Genova, Supramolecular organization of the mitochondrial respiratory chain: a new challenge for the mechanism and control of oxidative phosphorylation, Adv. Exp. Med. Biol. 748 (2012) 107–144.
[21] X. Tekpli, J.A. Holme, O. Sergent, D. Lagadic-Gossmann, Role for membrane remodeling in cell death: implication for health and disease, Toxicology 304 (2013) 141–157.
[22] N.C. Mykytczuk, J.T. Trevors, L.G. Leduc, G.D. Ferroni, Fluorescence polarization in studies of bacterial cytoplasmic membrane fluidity under environmental stress, Prog. Biophys. Mol. Biol. 95 (2007) 60–82.
[23] D.Z. He, J. Zheng, F. Kalinec, S. Kakehata, J. Santos-Sacchi, Tuning in to the amazing outer hair cell: membrane wizardry with a twist and shout, J. Membr. Biol. 209 (2006) 119–134.
[24] G.D. Chen, H.B. Zhao, Effects of intense noise exposure on the outer hair cell plasma membrane fluidity, Hear. Res. 226 (2007) 14–21.
[25] A.R. Fetoni, A. Ferraresi, C.L. Greca, D. Rizzo, B. Sergi, G. Tringalli, R. Piacentini, D. Troiani, Antioxidant protection against acoustic trauma by coadministration of idebenone and vitamin E, Neuroreport 19 (2008) 277–281.
[26] A.R. Fetoni, R. Piacentini, A. Fiorita, G. Paludetti, D. Troiani, Water-soluble coenzyme Q10 formulation (Q-ter) promotes outer hair cell survival in a guinea pig model of noise induced hearing loss (NIHL), Brain Res. 1257 (2009) 108–116.
[27] M.V. Podda, L. Leone, R. Piacentini, S. Cocco, D. Mezzogori, M. D'Ascenzo, C. Grassi, Expression of olfactory-type cyclic nucleotide-gated channels in rat cortical astrocytes, Glia 60 (2012) 1391–1405.
[28] J. Wang, R.V. Lloyd Faulconbridge, A. Fetoni, M.J. Guitton, R. Pujol, J.L. Puel, Local application of sodium thiosulfate prevents cisplatin-induced hearing loss in the guinea pig, Neuropharmacology 45 (2003) 380–393.
[29] J.V. Rocheleau, W.S. Head, D.W. Piston, Quantitative NAD(P)H/flavoprotein autofluorescence imaging reveals metabolic mechanisms of pancreatic islet pyruvate response, J. Biol. Chem. 279 (2004) 31780–31787.
[30] G.H. Patterson, S.M. Knobel, P. Arkhammar, O. Thastrup, D.W. Piston, Separation of the glucose-stimulated cytoplasmic and mitochondrial NAD(P)H responses in pancreatic islet beta cells, Proc. Natl. Acad. Sci. U. S. A. 97 (10) (2000) 5203–5207.
[31] T. Parasassi, E.K. Krasnowska, L. Bagatolli, E. Gratton, Laurdan and Prodan as polarity-sensitive fluorescent membrane probes, J. Fluoresc. 8 (1998) 365–373.
[32] G. Balogh, G. Maulucci, I. Gombos, I. Horváth, Z. Török, M. Péter, E. Fodor, T. Páli, S. Benko, T. Parasassi, M. De Spirito, J.L. Harwood, L. Vígh, Heat stress causes spatially-distinct membrane re-modelling in K562 leukemia cells, PLoS One 6 (2011) e21182.
[33] G. Maulucci, V. Labate, M. Mele, E. Panieri, G. Arcovito, T. Galeotti, H. Østergaard, J.R. Winther, M. De Spirito, G. Pani, High-resolution imaging of redox signaling in live cells through an oxidation-sensitive yellow fluorescent protein, Sci. Signal. 1 (2008) l3.
[34] G. Maulucci, G. Pani, V. Labate, M. Mele, E. Panieri, M. Papi, G. Arcovito, T. Galeotti, M. De Spirito, Investigation of the spatial distribution of glutathione redox-balance in live cells by using fluorescence ratio imaging microscopy, Biosens. Bioelectron. 25 (2009) 682–687.
[35] H.J. Kennedy, M.G. Evans, A.C. Crawford, R. Fettiplace, Depolarization of cochlear outer hair cells evokes active hair bundle motion by two mechanisms, J. Neurosci. 26 (2006) 2757–2766.
[36] P. Dallos, Cochlear amplification, outer hair cells and prestin, Curr. Opin. Neurobiol. 18 (2008) 370–376.
[37] J.S. Oghalai, H.B. Zhao, J.W. Kutz, W.E. Brownell, Voltage- and tension-dependent lipid mobility in the outer hair cell plasma membrane, Science 287 (2000) 658–661.
[38] L. Rajagopalan, J.N. Greeson, A. Xia, H. Liu, A. Sturm, R.M. Raphael, A.L. Davidson, J.S. Oghalai, F.A. Pereira, W.E. Brownell, Tuning of the outer hair cell motor by membrane cholesterol, J. Biol. Chem. 282 (2007) 36659–36670.

[39] J. Sfondouris, L. Rajagopalan, F.A. Pereira, W.E. Brownell, Membrane composition modulates prestin-associated charge movement, J. Biol. Chem. 283 (2008) 22473–22481.
[40] S. Takahashi, J. Santos-Sacchi, Non-uniform mapping of stress-induced, motility-related charge movement in the outer hair cell plasma membrane, Pflugers Arch. 441 (4) (2001) 506–513.
[41] C. Corbitt, F. Farinelli, W.E. Brownell, B. Farrell, Tonotopic relationships reveal the charge density varies along the lateral wall of outer hair cells, Biophys. J. 102 (12) (2012) 2715–2724.
[42] L.A. Tiede, P.S. Steyger, M.G. Nichols, R. Hallworth, Metabolic imaging of the organ of Corti — a window on cochlea bioenergetics, Brain Res. 1277 (2009) 37–41.
[43] R.F. Jacob, R.P. Mason, Lipid peroxidation induces cholesterol domain formation in model membranes, J. Biol. Chem. 280 (2005) 39380–39387.
[44] M.C. Holley, F. Kalinec, B. Kachar, Structure of the cortical cytoskeleton in mammalian outer hair cells, J. Cell Sci. 102 (Pt 3) (1992) 569–580.
[45] N. Matsumoto, R. Kitani, A. Maricle, M. Mueller, F. Kalinec, Pivotal role of actin depolymerization in the regulation of cochlear outer hair cell motility, Biophys. J. 99 (7) (2010) 2067–2076.
[46] S. Mahendrasingam, M. Beurg, R. Fettiplace, C.M. Hackney, The ultrastructural distribution of prestin in outer hair cells: a post-embedding immunogold investigation of low-frequency and high-frequency regions of the rat cochlea, Eur. J. Neurosci. 31 (2010) 1595–1605.
[47] L.F. Aguilar, J.A. Pino, M.A. Soto-Arriaza, F.J. Cuevas, S. Sánchez, C.P. Sotomayor, Differential dynamic and structural behavior of lipid-cholesterol domains in model membranes, PLoS One 7 (2012) e40254.
[48] W.E. Brownell, S. Jacob, P. Hakizimana, M. Ulfendahl, A. Fridberger, Membrane cholesterol modulates cochlear electromechanics, Pflugers Arch. 461 (2011) 677–686.
[49] O. Golfetto, E. Hinde, E. Gratton, Laurdan fluorescence lifetime discriminates cholesterol content from changes in fluidity in living cell membranes, Biophys. J. 104 (2013) 1238–1247.
[50] A.R. Fetoni, S.L. Eramo, R. Rolesi, D. Troiani, G. Paludetti, Antioxidant treatment with coenzyme Q-ter in prevention of gentamycin ototoxicity in an animal model, Acta Otorhinolaryngol. Ital. 32 (2012) 103–110.
[51] L.E. Van Campen, W.J. Murphy, J.R. Franks, P.I. Mathias, M.A. Toraason, Oxidative DNA damage is associated with intense noise exposure in the rat, Hear. Res. 164 (2002) 29–38.